

Statistical Asynchronous Regression: Determining the Relationship Between two Quantities that are not Measured Simultaneously

T.P. O'Brien¹, D. Sornette^{1,2,3} and R.L. McPherron^{1,2}

1. Institute of Geophysics and Planetary Physics, UCLA, Los Angeles, CA 90095

2. Department of Earth and Space Sciences, UCLA, Los Angeles, CA, 90095

3. Laboratoire de Physique de la Matière Condensée, CNRS and Université de Nice-Sophia

Antipolis, 06108 Nice Cedex 2, France

IGPP Publication No. 5471

October 29, 2018

Short title: STATISTICAL ASYNCHRONOUS REGRESSION

Abstract. We introduce the Statistical Asynchronous Regression (SAR) method: a technique for determining a relationship between two time varying quantities without simultaneous measurements of both quantities. We require that there is a time invariant, monotonic function $Y = u(X)$ relating the two quantities, Y and X . In order to determine $u(X)$, we only need to know the statistical distributions of X and Y . We show that $u(X)$ is the change of variables that converts the distribution of X into the distribution of Y , while conserving probability. We describe an algorithm for implementing this method and apply it to several example distributions. We also demonstrate how the method can separate spatial and temporal variations from a time series of energetic electron flux measurements made by a spacecraft in geosynchronous orbit. We expect this method will be useful to the general problem of spacecraft instrument calibration. We also suggest some applications of the SAR method outside of space physics.

1. Introduction

We developed the Statistical Asynchronous Regression (SAR) technique described in this paper as part of a study of relativistic electron conditions at geosynchronous orbit. This part of the Earth's radiation belts can evolve on a timescale of hours or even minutes. Unfortunately, while individual satellites may make measurements every few seconds, it is difficult to separate the temporal changes from consequences of orbital motion. The easiest way to do this would be to have continuous measurements at a fixed location, or local time, such as local noon. Instead, we have continuous measurements on board moving spacecraft. We can remove the orbital effects if we can map our continuous measurements to local noon at geosynchronous orbit.

Relativistic electrons in the vicinity of geosynchronous orbit drift around the earth every 5-15 minutes under the influence of the local magnetic field. As it happens, these electrons do not follow circular paths like satellite orbits, but rather elliptical paths that depend on the details of the local magnetic field geometry. However, because electron density is a relatively smooth function of altitude near geosynchronous orbit, measurements at different local times are strongly correlated. This correlation is stronger still if we average our data over several drift periods. The strong correlation suggests that we can map our continuous measurements to local noon, if we can determine the right mapping function.

Sometimes it is possible to determine empirical mappings between measurements at different local times by regression of simultaneous measurements. For example, it is possible to relate measurements made by the GOES 8 spacecraft at local dawn (0600) to GOES 9 measurements at local 10 AM (1000), because whenever GOES 8 is at local dawn, GOES 9 is at local 10 AM. However, it is never the case that GOES 8 is at local dawn when GOES 9 is at local noon. Therefore, we need some method for mapping measurements from anywhere to local noon (or some other local time of interest). Until recently, there have been three strategies for resolving this difficulty: interpolate between multiple calibrated spacecraft [Reeves *et al.*, 1998], use the equation of motion of electrons in model electromagnetic fields to follow particles around geosynchronous orbit [Friedel *et al.*, 1999], or use some kind of empirical description

of the orbital variations [Brautigam *et al.*, 1992; Vette, 1991]. The first approach degrades substantially when only a few spacecraft are available, and fails when only one spacecraft is available. The second approach suffers from the substantial imperfections in our magnetic field models near geosynchronous [Selesnick and Blake, 2000]. The third approach has been applied with encouraging success by Moorer [1999], who uses whatever measurements are available to adjust the CRRESELE empirical radiation belt model for best agreement. The SAR technique provides us with a more robust approach that can be applied in cases when there is no pre-existing empirical model like CRRESELE. The SAR technique calibrates not only between spacecraft and instruments but also between different locations (local times) around geosynchronous orbit. One can easily imagine the SAR technique as calibrating measurements made by GOES 8 at local dawn to measurements made by GOES 9 at local noon—even though these two spacecraft have never been at these locations simultaneously. Additionally, the SAR technique is non-parametric because it does not require us to assume a functional form for the mapping between local times.

When we have described the SAR technique to our colleagues, many have found it novel and challenging to understand, and some have stated that it might be useful in their own work on other problems. For our own purposes, since we have used this technique as the basis of a statistical study of the energetic electrons near geosynchronous orbit, we present this technique to familiarize our audience with the technique and to demonstrate its robustness. As we believe the SAR technique has applications beyond the electron radiation belts, we have chosen to dedicate this paper entirely to the technique itself, reserving the radiation belt study to a later publication.

In essence, our method provides a means of performing a regression of one time varying quantity against another without requiring simultaneous knowledge of both. We call this the Statistical Asynchronous Regression (SAR) method, because it allows us to regress $Y(t)$ against $X(t)$ using only the two statistical distributions $F(x)$ and $G(y)$. The SAR method determines the function $Y = u(X)$ by matching the quantiles (or percentiles) x and y of the distributions of X and Y for each probability level. A primitive variant of this technique was developed to standardize the calculation of K indices at different magnetic observatories

[Mayaud, 1980, and references therein]. We also note that a transformation similar to the SAR method has been introduced to map non-Gaussian random variables onto Gaussian ones, with application to the construction of multivariate distribution functions in high-energy particle physics experiments [Karlen, 1998], in the theory of portfolio in Finance [Sornette *et al.*, 2000], and earlier in the treatment of bivariate gamma distributions [Moran, 1969].

In statistics, one method of graphical hypothesis testing is the Q-Q (quantile-quantile) plot [Wilk and Gnanadesikan, 1968], which is essentially a graphical depiction of $u(X)$ based on the same principle as the SAR method. A linear $u(X)$ indicates that the two variables differ only by a scaling and an offset but are otherwise identically distributed. However, in spite of the variety of graphical techniques related to the SAR method, none makes use of the plotted $u(X)$, aside from determining whether it is linear [Fisher, 1983]. Since we are specifically interested in potentially nonlinear $u(X)$, we have developed the SAR method as an extension to the Q-Q plot.

Under various names, such as *anchoring* or the *equipercentile* method, psychological and educational testing use the same principle as the SAR technique to normalize a new test to a standard score distribution [Allen and Yen, 1979]. However, $u(X)$ is not explicitly calculated, and the information it contains is typically discarded.

Additionally, the Spearman rank order correlation coefficient touches on the same notion as the SAR method [Press *et al.*, 1992]. It calculates a linear correlation coefficient between the sorted rank orders of two quantities rather than the quantities themselves; this coefficient measures the quality of the optimal nonlinear mapping between two simultaneously measured quantities. Since we are concerned with comparing quantities not measured simultaneously, we will not make use of the Spearman coefficient.

In the remainder of this paper, we will provide a description and some limited analysis of the SAR method. First, we will describe the technique by parable, using a graphical illustration. Next we will provide the formal derivation of the technique. We will provide several examples and a simple recipe for the implementation of the SAR technique. Then we will address the problems of finite sample size and noisy measurements. Finally we will show how we use the SAR method to map geosynchronous energetic electron flux from one local

time to another.

2. A Simple Example

We begin our explanation of the SAR technique by taking a step back from space physics to a simpler analogous problem. Suppose we have two meteorologists making measurements every other day. One has been measuring his favorite meteorological quantity X , and the other has been measuring Y . Unfortunately, owing to an error in scheduling, the two meteorologists have not been making their measurements on the same days. It is therefore impossible for them to plot Y against X and perform a regression. We will show how it is nonetheless possible for them to recover the empirical function $Y = u(X)$. The powerful statistical tool that will make this possible is the fundamental principle that probability is conserved under a change of variables. We will leave the mathematical presentation of this principle to later sections.

In Figure 1, we have plotted the probability density functions (PDFs) $f(x)$ and $g(y)$ along the x - and y -axes respectively. For clarity, we have plotted $f(x)$ upside down and $g(y)$ rotated counterclockwise. Each density function represents the distribution of observations made by one of the scientists. In this example, X is distributed uniformly between 1 and 2, and Y is distributed as $1/y$ between e and e^2 . We have also plotted the relational function $Y = u(X) = e^X$ that provides the change of variables. The shaded area within $f(x)$ is the probability that a single measurement of X falls between x_1 and x_2 . Similarly, the shaded area within $g(y)$ is the probability that a single measurement of Y falls between $y_1 = u(x_1)$ and $y_2 = u(x_2)$. The conservation of probability is illustrated graphically by the fact that the two shaded regions are equal in area. With any two of these three curves, it is possible to determine the third. Generally, it has been of greater interest to reconstruct $g(y)$ knowing $f(x)$ and $u(X)$. We, however, are interested in reconstructing $u(X)$ knowing only $f(x)$ and $g(y)$. The fundamental assumption is that of stationarity: the unknown relationship $Y = u(X)$ is the same at all times; this condition must be met for a statistical approach to be possible.

Figure 1

One can reconstruct $Y = u(X)$ for each X simply by finding the value Y such that the

area inside $g(y)$ from $-\infty$ to Y is equal to the area inside $f(x)$ from $-\infty$ to X . In Figure 2 we demonstrate this cumulative way of looking at the problem. Instead of plotting the density functions $f(x)$ and $g(y)$, we have plotted the cumulative distribution functions (CDFs) $F(x)$ and $G(y)$. The CDFs are the integrals from $-\infty$ to x of $f(x)$ and $-\infty$ to y of $g(y)$, and they correspond to the areas inside $f(x)$ and $g(y)$ mentioned above. To find the Y that corresponds to a given X in Figure 2, one reads from the X value on the abscissa up to $F(x)$ then horizontally over to the same value of $G(y)$, and back down to the abscissa to find the corresponding Y . Compared to Figure 1, this visualization makes it easier to find Y for a given X , but does not provide an obvious representation of $u(X)$. While emphasizing different features of the method, these two graphical representations of the method give identical results. In the following sections, we will provide the formal mathematical treatment of the graphical operations.

Figure 2

3. Formalism

Some of our readers will no doubt be a bit rusty in the manipulation of probabilities. Therefore, we have included a thorough treatment of the change of variables theorem in an appendix. Here, we begin with the differential form of the change of variables:

$$\begin{aligned} f(x)dx &= g(u(x))|u'(x)|dx \\ &= g(y)\left|\frac{dy}{dx}\right|dx = g(y)|dy|. \end{aligned} \tag{1}$$

In order to use this equation, we must determine the sign of $u'(x)$. For distributions with only one tail, we can do this rather easily by examining the rare values of X and Y . When the rare values of X and Y fall at the same end of the real number line, $u'(x)$ is positive. When they fall at opposite ends, $u'(x)$ is negative. Physical insight is also a useful tool in determining the sign of $u'(x)$. If we expect larger (or more positive) values of X to correspond to larger values of Y , then $u'(x)$ is positive. If we expect larger values of X to correspond to smaller (or more negative) values of Y , then $u'(x)$ is negative.

For $u'(x) > 0$, we can integrate (1),

$$\int_{-\infty}^x f(x')dx' = \int_{-\infty}^y g(y')dy'. \quad (2)$$

This equation implicitly defines $y = u(x)$ as the function that provides the matching integration bounds. We recognize these integrals as the CDFs of X and Y , so we can rewrite (2) as

$$F(x) = G(y) \text{ for } u'(x) > 0. \quad (3)$$

We can invert $G(y)$ to arrive at an explicit equation for $u(x)$,

$$y = G^{-1}(F(x)) = u(x). \quad (4)$$

This equation represents the mathematical counterpart to the graphical operation described in Figure 2, where one moves up from X to $F(x)$, then across to $G(y)$, then back down to the corresponding Y .

For $u'(x) < 0$, we can integrate (1),

$$\int_{-\infty}^x f(x')dx' = \int_y^{+\infty} g(y')dy'. \quad (5)$$

Converting this equation to CDFs, we have

$$F(x) = 1 - G(y) \text{ for } u'(x) < 0. \quad (6)$$

solving for $u(x)$, we arrive at

$$y = G^{-1}(1 - F(x)) = u(x). \quad (7)$$

Combining (4) and (7) we arrive at

$$u(x) = \begin{cases} G^{-1}(F(x)) & \text{for } u'(x) > 0, \\ G^{-1}(1 - F(x)) & \text{for } u'(x) < 0. \end{cases} \quad (8)$$

It is clear, then, that all we need to determine $u(x)$ is knowledge of the sign of $u'(x)$ and either $F(x)$ and $G(y)$ or $f(x)$ and $g(y)$. We summarize the desirable properties of $u(x)$ as follows:

- it can be arbitrarily nonlinear;
- its determination is not parametric;
- it maps the entire distribution and all of the moments of X onto those of Y ;
- it can be determined without simultaneous measurements of X and Y .

4. More Examples

We now turn to some more sophisticated examples of the SAR method. First, we will return to our original meteorological example to demonstrate the SAR procedure on analytical functions. Then, we will provide a function relating a bimodal distribution to a Gaussian. Finally, we will demonstrate the method on a stretched exponential and a Gaussian.

4.1. Meteorological Example

In the example of the meteorologists, illustrated in Figures 1 and 2, the following analytical functions were used:

$$f(x) = \begin{cases} 1 & \text{for } 1 \leq x < 2, \\ 0 & \text{otherwise,} \end{cases} \quad (9)$$

$$g(y) = \begin{cases} 1/y & \text{for } e \leq y < e^2, \\ 0 & \text{otherwise.} \end{cases} \quad (10)$$

Using (A3) and (A4) together with (9) and (10), we have

$$F(x) = \begin{cases} 0 & \text{for } x < 1, \\ x - 1 & \text{for } 1 \leq x < 2, \\ 1 & \text{for } x \geq 2, \end{cases} \quad (11)$$

$$G(y) = \begin{cases} 0 & \text{for } y < e, \\ \log y - 1 & \text{for } e \leq y < e^2, \\ 1 & \text{for } y \geq e^2. \end{cases} \quad (12)$$

Inserting (11) and (12) into (4), we see that

$$u(x) = G^{-1}(F(x)) = e^{1+F(x)} = e^x. \quad (13)$$

Adding in the proper bounds, we have

$$u(x) = e^x \text{ for } 1 \leq x < 2. \quad (14)$$

4.2. Bimodal Example

In our next example, we will show how the SAR method easily handles bimodal distributions. We have chosen X to be bimodal and Y to be unimodal. The PDFs are

$$f(x) = \frac{1}{2\sqrt{2\pi}} \left(e^{-\frac{1}{2}(x-3)^2} + e^{-\frac{1}{2}(x-8)^2} \right), \quad (15)$$

$$g(y) = \frac{1}{3\sqrt{2\pi}} e^{-\frac{1}{2}\left(\frac{y-10}{3}\right)^2}. \quad (16)$$

While there is no closed form for $u(X)$, a graphical display can show its qualitative features. Figure 3 shows how the bimodal $f(x)$ maps to $g(y)$. The highly nonlinear mapping $u(X)$ has a flat spot (with small but still positive slope) corresponding to the local minimum in $f(x)$, since $u'(x) = f(x)/g(u(x))$. In Figure 3, we see how a large range of X values near $X = 5$ maps to a very narrow range of Y values near $Y = 10$. More generally, the terraced shape of $u(X)$ can be seen to generate bimodal or multimodal distributions from unimodal ones.

Figure 3

4.3. Stretched Exponential Example

For our final example, we will treat an unusual distribution and an unusual mapping. We consider the case of a stretched exponential mapped to a Gaussian. In this case, X and Y are distributed as

$$f(x) = \frac{c}{\sqrt{\pi x_0}} \left(\frac{x}{x_0} \right)^{\frac{c}{2}-1} e^{-\left(\frac{x}{x_0} \right)^c} \text{ for } x > 0, \quad (17)$$

$$g(y) = \sqrt{\frac{2}{\pi\sigma^2}} e^{-\frac{(y-\mu)^2}{2\sigma^2}} \quad \text{for } y > \mu, \quad (18)$$

where c , σ , and x_0 are positive real values. Using (1) and assuming $u'(x) > 0$, we can write a differential equation for $u(x)$,

$$\frac{c}{\sqrt{\pi}x_0} \left(\frac{x}{x_0}\right)^{\frac{c}{2}-1} e^{-\left(\frac{x}{x_0}\right)^c} = \sqrt{\frac{2}{\pi\sigma^2}} e^{-\frac{(u(x)-\mu)^2}{2\sigma^2}} u'(x). \quad (19)$$

By our design of (17), $u(x)$ will cause the two exponentials to drop out of the equation, satisfying the system

$$-\left(\frac{x}{x_0}\right)^c = -\frac{(u(x)-\mu)^2}{2\sigma^2}, \quad (20)$$

$$\frac{c}{\sqrt{\pi}x_0} \left(\frac{x}{x_0}\right)^{\frac{c}{2}-1} = \sqrt{\frac{2}{\pi\sigma^2}} u'(x). \quad (21)$$

Solving (20) for $u(x)$ we have

$$u(x) = \sqrt{2}\sigma \left(\frac{x}{x_0}\right)^{\frac{c}{2}} + \mu, \quad (22)$$

which is, in fact, the solution to (21) and thus of (19). This mapping function is a highly nonlinear power-law. In Figure 4, we have depicted the borderline case for $c = 1$, $x_0 = 1$, $\sigma = 1/\sqrt{2}$ and $\mu = 0$. For $c < 1$, this distribution becomes a stretched exponential, which is a common distribution in real data. While $f(x)$ diverges at $x = 0$, the SAR method cleanly recovers the mapping function $u(x) = 2\sqrt{x}$. We are now going to investigate the robustness of the SAR method on finite and noisy data sets.

Figure 4

5. The Algorithm and Associated Approximation Problems

So far, we have considered the analytical representations of $f(x)$ and $g(y)$. However, in practice, we will only have a finite number of samples of each variable. We can use these samples to construct $F(x)$ and $G(y)$ and then perform either a tabular or an analytical approximation to (8).

First, we sort the X and Y values. These sorted values give us an approximation to $F(x)$ and $G(y)$. For example, if x_i is the i^{th} smallest value in N_x measurements of X , then an

estimate of $F(x)$ is

$$F^*(x_i) = \frac{i}{N_x}. \quad (23)$$

Similarly, we estimate $G(y)$ as

$$G^*(y_j) = \frac{j}{N_y}. \quad (24)$$

There are more sophisticated methods of estimating these distributions, such as kernel estimators [Hardle, 1990], if the need arises.

Henceforth, we will only treat the case $u'(X) > 0$, but the interested reader can easily derive the $u'(X) < 0$ case in a similar fashion. To obtain $u(X)$ for a particular X , we find i such that

$$x_i \leq X < x_{i+1}. \quad (25)$$

Next we find j_1 and j_2 such that

$$G^*(y_{j_1}) \leq F^*(x_i) < G^*(y_{j_1+1}), \quad (26)$$

$$G^*(y_{j_2}) \geq F^*(x_{i+1}) > G^*(y_{j_2-1}). \quad (27)$$

We then have an estimate of Y

$$Y \approx \frac{y_{j_1} + y_{j_2}}{2}. \quad (28)$$

By determining a Y for each sample of X , we achieve a tabular definition of $Y = u(X)$. We have depicted the mapping process and the uncertainty for the bimodal example in Figure 5. We have chosen artificially small datasets of $N_x = 15$ and $N_y = 25$ to illustrate the estimation effect.

Figure 5

The approximate uncertainty Δy in the Y estimated from (28) is given by

$$\Delta y \approx \frac{y_{j_2} - y_{j_1}}{2}. \quad (29)$$

We can rewrite (29) in terms of G^{*-1} as

$$\begin{aligned} \Delta y &\approx \frac{G^{*-1}(j_2/N_y) - G^{*-1}(j_1/N_y)}{2} \\ &= \frac{j_2 - j_1}{2N_y} \frac{G^{*-1}(j_2/N_y) - G^{*-1}(j_1/N_y)}{(j_2 - j_1)/N_y}. \end{aligned} \quad (30)$$

This expression contains a first order estimate of the derivative of G^{*-1} which, using (A4), can be expressed in terms of $g(y)$ as

$$\begin{aligned} \frac{G^{*-1}(j_2/N_y) - G^{*-1}(j_1/N_y)}{(j_2 - j_1)/N_y} &\approx D(G^{*-1}) \\ &\approx D(G^{-1}) = \left(\frac{dG}{dy}\right)^{-1} = \frac{1}{g(y)}. \end{aligned} \quad (31)$$

Therefore (30) can be expressed as

$$\Delta y \approx \frac{j_2 - j_1}{2N_y g(\frac{y_{j_1} + y_{j_2}}{2})}. \quad (32)$$

Rewriting (26) and (27) using (23) and (24), we have

$$\frac{j_1}{N_y} \leq \frac{i}{N_x}, \quad (33)$$

$$\frac{j_2}{N_y} \geq \frac{i+1}{N_x}. \quad (34)$$

Therefore

$$j_2 - j_1 \geq \frac{N_y}{N_x}, \quad (35)$$

which leads us to

$$\Delta y \gtrsim \frac{1}{2g(\frac{y_{j_1} + y_{j_2}}{2})N_x} = \frac{1}{2g(y)N_x}. \quad (36)$$

Here, N_x accounts for the sampling effect. This relationship implies that in the rarified regions of the Y distribution, where $g(y)$ is small, the estimation error is large. It also suggests that, to first order, increasing the Y sample size N_y is not as useful in reducing Δy as would be increasing the X sample size N_x . However, the uncertainty in x is also important because the total uncertainty in x - y space is $\Delta x \Delta y$. By a derivation similar to that of Δy , we have

$$\Delta x \gtrsim \frac{1}{2f(x)N_y}, \quad (37)$$

for a total uncertainty of

$$(2\Delta x)(2\Delta y) \gtrsim \frac{1}{f(x)g(y)N_x N_y}. \quad (38)$$

To improve the overall quality of the reconstruction of $Y = u(X)$, we would like both N_x and N_y to be as large as possible.

6. The SAR on Noisy Data

Another consideration for the implementation of the SAR method is the effect of noise. Until now, we have assumed that there is no noise in our measurements of X and Y . However, in practice, we always encounter noisy data, and we want to be sure that the SAR does not become invalid under typically noisy conditions. In a standard regression, where simultaneous values of X and Y are known, a least-squares approach can be used to determine $u(X)$ from noisy X and Y . We will attempt to demonstrate the effect of noise on the SAR method by simulating a noisy version of the meteorological example. We generate 100 noisy samples from the distributions $f(x)$ and $g(y)$ given in (9) and (10). The noise distributions are chosen to be unbiased Gaussians with standard deviations η_x and η_y for X and Y . For now, we choose η_x and η_y to be 25% of the standard deviations σ_x and σ_y of X and Y . We can fit the noisy data with $\log Y = \alpha X + \log \beta$. We perform two such fits: a standard least-squares regression on the $(X, \log Y)$ pairs and least-squares regression on the $(X, \log u(X))$ pairs produced by the SAR method described in (28). For this parametric example, a maximum likelihood estimation of α and β would probably outperform the least-squares approach, but we will compare to the more familiar regression for this illustration.

Ideally, $\alpha = 1$ and $\beta = 1$, but, for the noisy data, the two regressions give

$$u(x) = 1.21e^{0.88x} \quad \text{Standard Regression,} \quad (39)$$

$$u(x) = 1.14e^{0.92x} \quad \text{SAR.} \quad (40)$$

The SAR fit is significantly better than the standard regression. In the future, it would be interesting to study how this depends on the type of noise and the form of $u(X)$. In Figure 6, we see a graphical depiction of the noisy data and the two fits. Both fits lie very close to the true $u(X)$ curve compared to the noisy data, however there is a clear improvement with the SAR fit.

Figure 6

To understand better the effect of noise, we repeat the above simulation 5000 times to obtain a distribution of α for each fitting approach. These distributions are plotted in Figure 7. It is clear that both methods provide biased estimates of α . The SAR method produces a smaller bias, but we would still like to know how that bias depends on the noise amplitude.

Figure 7

We can test this dependence by finding the bias for various noise/signal ratios r . We will choose the same r for X and Y , such that

$$r = \frac{\eta_x}{\sigma_x} = \frac{\eta_y}{\sigma_y}. \quad (41)$$

So far, we have only tested $r = 0.25$, but now we will test a full range from $r = 0$ to $r = 1.2$.

In Figure 8, we have plotted the median estimated α versus r . We see that for small noise, the estimate quality is high, but, as r approaches 1, the estimation fails. The α estimated by the SAR method is generally of higher quality than the estimate from the standard regression. For relatively large noise amplitude neither regression method produces quality estimates of α . It is clear that, while the derivation of the SAR method assumes noiseless data, our implementation of the SAR method is at least as robust to noise as is the traditional least-squares regression. The SAR appears to be reliable when the noise amplitude is small compared to the variability of the data sample.

Figure 8

7. An Example from Space Physics

Finally, we would like to demonstrate the SAR method on a real problem from space physics. The GOES 8 geosynchronous spacecraft measures, among other things, the flux of electrons with energies above 2 MeV. The spacecraft orbits the Earth once per day. The electron populations at geosynchronous orbit are organized by the position of the Sun relative to the Earth, which we identify as local time. Owing to the asymmetry of the Earth's magnetic field in space, as the spacecraft passes through different local times, it measures slightly different parts of the radiation belts. Because the relativistic electron density varies smoothly with altitude and the electrons themselves make slightly elliptical orbits every few minutes, hour averaged fluxes at all locations around geosynchronous orbit are well correlated [Li *et al.*, 1997]; we therefore expect a monotonically increasing function $Y = u(X)$ relating fluxes X measured at one local time lt_x to fluxes Y measured at another local time lt_y . We can estimate the flux at lt_y from a measurement made by the spacecraft at lt_x if we can determine $u(X)$. The probability distributions of electron measurements at every local time at geosynchronous are relatively stationary in time; that is, the distribution of measurements in one year is

roughly equivalent to the distribution of measurements in any other year. Therefore, we can estimate $F(x)$ and $G(y)$ using historical measurements of X and Y , and we can use the SAR method to reconstruct $u(X)$. We will assume lt_x is local dawn and lt_y is local noon.

We have obtained GOES 8 measurements for 1998 from CDAWeb (<http://cdaweb.gsfc.nasa.gov/>) [McGuire *et al.*, 2000]. We calculated hourly averages and grouped them into 1-hour bins near local dawn and local noon. This gives us about 360 samples at each location, but none that are simultaneous because the spacecraft is only at one location at a time. Because electron measurements tend to be heavily biased toward low values, we will use the Complementary Cumulative Distribution Functions $F_>(x) = 1 - F(x)$ and $G_>(y) = 1 - G(y)$. In terms of these functions, for a monotonically increasing $u(X)$, we have

$$u(x) = G^{-1}(F(x)) = G_>^{-1}(F_>(x)). \quad (42)$$

Figure 9 shows the constructed $F_>^*(x)$ and $G_>^*(y)$. We can fit both distributions with the same analytical form:

Figure 9

$$F_>^*(x) \approx e^{-\sqrt{\frac{x}{307}}} \quad (\text{Dawn}), \quad (43)$$

$$G_>^*(y) \approx e^{-\sqrt{\frac{y}{533}}} \quad (\text{Noon}). \quad (44)$$

Assuming an increasing $u(X)$, we use (42) to arrive at an analytical form for $u(X)$:

$$\begin{aligned} u(X) &= G_>^{*-1}(F_>^*(x)) \\ &= 533(-\log F_>^*(X))^2 = \frac{533}{307}X \\ &= 1.74X. \end{aligned} \quad (45)$$

The non-parametric SAR mapping is shown in Figure 10 to be nearly a power-law. We have determined an analytical fit to be

Figure 10

$$Y = u(X) = (1.8 \pm 0.4)X^{1.00 \pm 0.04}. \quad (46)$$

This fit is in agreement with the function $u(X) = 1.74X$ derived in (45) above from the implementation of the SAR method using the parameterizations (43) and (44) of the cumulative distributions.

The fact that the exponent in (46) is very nearly 1 indicates that the densities at dawn and noon change in fixed proportion to each other, even as the radiation belts are filled during geomagnetic activity. If we imagine the electron phase-space structure to be $f(\vec{r}, \vec{v}, t)$, then we can state the proportionality as

$$f(\vec{r}_1, \vec{v}_1, t) \propto f(\vec{r}_2, \vec{v}_2, t). \quad (47)$$

This relationship suggests a simple separation of variables:

$$f(\vec{r}, \vec{v}, t) = \tilde{f}(\vec{r}, \vec{v})N(t), \quad (48)$$

where $\tilde{f}(\vec{r}, \vec{v})$ represents a phase space shape function, and $N(t)$ represents the varying global relativistic electron content of the geosynchronous region.

The parameterizations (43) and (44) together with the corresponding prediction (45) validated by the direct non-parametric implementation of the SAR method giving (46) suggest in addition a simple and useful representation of the heavy tail structure of the distribution of electron fluxes in terms of stretched exponentials. Such distributions have been found to parameterize a large variety of distributions found in nature as well as in social sciences [Laherrère and Sornette, 1998]. They present a quasi-stable property [Sornette et al., 2000; Sornette, 2000] and can be shown to be the generic result of the product of random variables in the “extreme deviation” regime [Frisch and Sornette, 1997].

So far, we have only determined the mapping from local dawn to local noon. It may also be necessary to allow $u(X)$ to vary with magnetic activity level. The magnetic indices Dst and Kp measure the intensity of the magnetospheric ring current and the variability of magnetospheric currents, respectively [Mayaud, 1980]. We can create different mappings $u(X; Dst, Kp)$ for each of several bins of geomagnetic indices; such binning would organize the data by the state of the system, reinforcing the assumption that each $u(X; Dst, Kp)$ is monotonic and time invariant. Using the SAR method, we can find mapping functions from every local time to every other local time, depending on geomagnetic activity, as necessary; this allows us to reconstruct the flux around the entire orbit at any time based only on the single measurement made by GOES 8. If we produce fluxes around the entire orbit every

hour, we can view spatial and temporal variations separately. In particular, if we reconstruct a time series of hourly fluxes at a fixed local time, we can perform various time series analyses that will not be influenced by the spatial variations seen in the measured time-series. This investigation will be reported elsewhere.

8. Discussion

We have shown that it is possible to accurately determine the function relating two variables even when they are not measured simultaneously. Specifically, we were trying to map energetic electron fluxes between different local times at geosynchronous orbit. However, we believe that our solution may be useful to other researchers whose data are not taken simultaneously. We developed a technique, Statistical Asynchronous Regression (SAR), that uses the statistical distributions of two variables to determine the unique monotonic function that can map one distribution onto the other. Because the SAR technique only works when there is a monotonic relationship between the two quantities, it should only be applied to quantities that are believed to be highly correlated with each other. We caution that the SAR technique will produce a relationship for any two quantities, regardless of whether they are actually related. It is particularly inappropriate to use the SAR to describe chaotic systems, which generally arise from non-monotonic behaviors. Also, when the noise amplitude is a substantial fraction of the data sample variability, we do not expect the SAR to give reliable results.

To illustrate the SAR technique when the two distributions are known analytically, we have provided several examples of common distributions. We have shown that the SAR technique can recover the underlying relationship of the two quantities even when one distribution diverges or has more than one local maximum. We have provided a simple algorithm for implementing the SAR. We derived simple expressions for the uncertainty in the estimated relationship between the two quantities. To ensure that the technique is robust for noisy data, we have simulated two noisy variables with a known relationship and determined how well the SAR technique recovers that relationship; the SAR performs better than a least squared

error regression, which requires simultaneous measurements of both quantities. While we expect that ultimately most scientists will wish to fit $u(X)$ to some parametric form, we feel that it is important that the SAR does not require us to assume a parametric form a priori.

For those wishing to apply the SAR technique to problems where $u'(X)$ passes through zero, we offer the following strategy: if the $u'(X) = 0$ occurs at known X and Y , then the SAR technique is perfectly valid in bins of X and Y constrained to be between the zeros of $u'(X)$. In this way, the SAR would provide a piecewise form of $u(X)$.

In closing, we would like to suggest some areas that might benefit from the SAR approach. In modeling tectonic deformations, it is useful to quantify the balance of deformation accommodated by different faults in a complex network [Cowie and Scholz, 1992]. For an individual fault, we often can measure only its length or its offset. Relying only on faults with both length and offset known would exclude many useful measurements. However, the physics of tectonic deformation leads us to expect a monotonic relationship between fault length and offset. In this case, the SAR technique would allow us to regress fault length against fault offset, using all of the available measurements. Similarly, for individual earthquakes we often know only one of seismic moment and energy released [Mayeda and Walter, 1996]; the SAR technique would allow us to regress all the available measurements rather than only those from earthquakes with both moment and energy known. We hope that the ideas presented here will assist those who need to relate non-simultaneous measurements.

Appendix: The Change of Variables Theorem

The SAR method relies heavily on the change of variables theorem from probability theory. The following derivation will be instructive to those not familiar with the manipulation of probabilities.

We will use the notational style $P[X \leq x]$ to denote the probability that any sample from the population of X will be less than or equal to some threshold x . The formal definitions of the probability density functions (PDFs) and cumulative distribution functions (CDFs) for X and Y are:

$$f(x)dx = P[x \leq X < x + dx], \quad (\text{A1})$$

$$g(y)dy = P[y \leq Y < y + dy], \quad (\text{A2})$$

$$F(x) = P[X \leq x] = \int_{-\infty}^x f(x')dx', \quad (\text{A3})$$

$$G(y) = P[Y \leq y] = \int_{-\infty}^y g(y')dy'. \quad (\text{A4})$$

By definition $f(x)$ and $g(y)$ are non-negative, and $F(x)$ and $G(y)$ reach 1 at $+\infty$. For most purposes, $f(x)$ and $g(y)$ are finite, continuous functions, and we will operate under that assumption. Accordingly, $F(x)$ and $G(y)$ are monotonically increasing, invertible functions.

We assume there is a continuous function $u(X)$ that provides the Y that corresponds to a given X ,

$$Y = u(X). \quad (\text{A5})$$

We will occasionally replace Y and X with y and x , but this should not worry the reader, as the function u has the same meaning regardless of its argument. This function must also be monotonic:

$$u'(X) \neq 0 \text{ for all } X. \quad (\text{A6})$$

Not only does this imply that $u(X)$ is unique and invertible, but it also implies that the sign of $u'(X)$ must be either always positive or always negative. Strictly speaking, $u'(X)$ may vanish at isolated points, so long as it only touches, but does not traverse, zero.

We can write $u'(x)$ as

$$u'(x) = \lim_{\Delta x \rightarrow 0} \frac{u(x + \Delta x) - u(x)}{\Delta x}. \quad (\text{A7})$$

If $u'(x)$ is positive for all values of x , then $\Delta x > 0$ implies that $u(x + \Delta x) > u(x)$. Formally, with $x + \Delta x$ replaced by X , we state this as

$$u'(x) > 0 \iff \{X > x \iff u(X) > u(x)\}. \quad (\text{A8})$$

By similar reasoning,

$$u'(x) < 0 \iff \{X > x \iff u(X) < u(x)\}. \quad (\text{A9})$$

For the case $u'(x) > 0$, we can therefore replace the inequality in (A3) according to (A8) to arrive at

$$F(x) = P[X \leq x] = P[u(X) \leq u(x)]. \quad (\text{A10})$$

Using (A4) and (A5), we have

$$F(x) = P[Y \leq u(x)] = G(u(x)). \quad (\text{A11})$$

For the other case, $u'(X) < 0$, we can use (A9) similarly to replace the inequality in (A3), which gives

$$\begin{aligned} F(x) &= P[X \leq x] = P[u(X) \geq u(x)] \\ &= 1 - P[u(X) < u(x)]. \end{aligned} \quad (\text{A12})$$

For a finite, continuous distribution $f(x)$, $P[u(X) < u(x)] = P[u(X) \leq u(x)]$. Therefore, we can apply (A4) and (A5) to (A12) to arrive at

$$F(x) = 1 - P[Y \leq u(x)] = 1 - G(u(x)). \quad (\text{A13})$$

By differentiating (A11) and (A13), we arrive at

$$f(x)dx = g(u(x)) u'(x)dx \quad \text{for } u'(x) > 0, \quad (\text{A14})$$

$$f(x)dx = -g(u(x)) u'(x)dx \quad \text{for } u'(x) < 0, \quad (\text{A15})$$

or, equivalently,

$$\begin{aligned} f(x)dx &= g(u(x))|u'(x)|dx \\ &= g(y) \left| \frac{dy}{dx} \right| dx = g(y)|dy|. \end{aligned} \quad (1)$$

Probability is conserved under a change of variables. This is the change of variables theorem, and it is depicted graphically in Figure 1.

Acknowledgments. This work was in part funded by IGPP grant LANL 1001 and NSF grant ATM 98-19935. We would like to thank G. Reeves and the Energetic Particles group at Los Alamos National Lab for their insightful critique of preliminary presentations of the

SAR method. We would also like to thank CDAWeb and T. Onsager for providing data from the GOES 8 spacecraft. We thank V. Pisarenko, F. Schoenberg, and A. Russell for helpful comments on the technique and manuscript. IGPP No. 5471.

References

- Allen, M.J., and W.M. Yen, *Introduction to measurement theory*, Brooks/Cole Publishing, Monterey, CA, 1979.
- Brautigam, D.H., M.S. Gussenhoven, and E.G. Mullen, Quasi-static Model of Outer Zone Electrons, *IEEE Trans. Nucl. Sci.*, *39*, 1797-1803, 1992.
- Cowie, P.A. and C.H. Scholz, Displacement length scaling relationship for faults – Data synthesis and discussion, *J. Struct. Geol.* *14*, 10:1149-1156, 1992.
- Fisher, N. I., Graphical methods in nonparametric statistics: a review and annotated bibliography, *International Statistical Review* *51*, 25-58, 1983.
- Friedel, R.H.W., G. Reeves, D. Belian, T. Cayton, C. Mouikis, A. Korth, B. Blake, J. Fennell, S. Selesnick, D. Baker, T. Onsager, and S. Kanekal, A multi-spacecraft synthesis of relativistic electrons in the inner magnetosphere using LANL, GOES, GPS, SAMPEX, HEO, and POLAR, *Radiation Measurements* *30*, 589-597, 1999.
- Frisch, U. and D. Sornette, Extreme deviations and applications, *J. Phys. I France* *7*, 1155-1171, 1997.
- Hardle, W., *Applied nonparametric regression*, *Econometric Society Monogr.*, Cambridge University Press, New York, 1990.
- Karlen, D., Using projections and correlations to approximate probability distributions, *Computer in Physics* *12*, 380-384, 1998.
- Laherrère, J. and D. Sornette, Stretched exponential distributions in Nature and Economy: “Fat tails” with characteristic scales, *European Physical Journal B* *2*, 525-539, 1998.
- Li, Xinlin, D.N. Baker, M. Temerin, T.E. Cayton, E.G.D. Reeves, R.A. Christensen, J.B.

- Blake, M.D. Looper, R. Nakamura, and S.G. Kanekal, Multisatellite observations of the outer zone electron variation during the November 3-4, 1993 magnetic storm, *J. Geophys. Res.*, *102*, 14,123-14,140, 1997.
- Mayaud, P.N., *Derivation, meaning and use of geomagnetic indices*, *Geophys. Monogr. Ser.*, vol. 22, American Geophysical Union, Washington, D.C., 1980.
- Mayeda, K. and W.R. Walter, Moment, energy, stress drop and source spectra of western United States earthquakes from regional coda envelopes, *J. Geophys. Res.*, *101*, B5:11195-11208, 1996.
- Moorer, D., Specifying outer belt electrons by data assimilation, Spring AGU Meeting, 1999.
- McGuire, R.E., R.J. Burley, R.M. Candey, R.L. Kessel, T.J. Kovalick, CDAWeb and SSCWeb: Enabling correlative international sun-earth-connections science entering the era of IMAGE and Cluster, Spring AGU Meeting, 2000.
- Moran, P.A.P., Statistical inference with bivariate gamma distributions, *Biometrika* *56*, 627-634, 1969.
- Press, W.H., S.A. Teukolsky, w.T. Betterling, B.P. Flannery, *Numerical Recipes in C: The Art of Scientific Computing*, Cambridge University Press, Cambridge, MA, 1992.
- Reeves, G. D., D. N. Baker, R. D. Belian, J. B. Blake, T. E. Cayton, J. F. Fennell, R. H. W. Friedel, M. M. Meier, R. S. Selesnick, and H. E. Spence, The global response of relativistic radiation belt electrons to the January 1997 magnetic cloud, *Geophys. Res. Lett.*, *25*, 3265-3268, 1998.
- Selesnick, R.S. and J.B. Blake, On the source location of radiation belt relativistic electrons, *J. Geophys. Res.*, *105*, 2607-2624, 2000.

Sornette, D., *Critical Phenomena in Complex Systems, Concepts and Tools for Variability at Many Scales* (Springer, Heidelberg, 2000)

Sornette, D., P. Simonetti, and J.V. Andersen, ϕ^q -field theory for Portfolio optimization: “fat tails” and non-linear correlations, *Physics Reports*, 335, 19-92, 2000.

Vette, J., The AE-8 trapped electron model environment, National Space Science Data Center, Report 91-24, Greenbelt, Maryland, 1991.

Wilk, M.B. and R. Gnanadesikan, Probability plotting methods for the analysis of data, *Biometrika* 55, 1-17, 1968.

T.P. O’Brien, D. Sornette, R. L. McPherron, Institute of Geophysics and Planetary Physics, UCLA, 405 Hilgard, Los Angeles, CA 90095-1567, tpoiii@igpp.ucla.edu, sornette@moho.ess.ucla.edu, rmcpherr@igpp.ucla.edu

Received 2000; revised 2000; accepted 2000.

Figure 1. Probability densities for X and Y are plotted outside the respective axes. The relational function $Y = u(X)$ provides the scaling from X to Y . Consistent with the conservation of probability, the shaded regions have equal area.

Figure 2. Cumulative distribution functions are plotted for X and Y on the horizontal axis. Following the dashed line, one can easily determine what value of Y corresponds to a given X .

Figure 3. In the same format as Figure 1, this is a depiction of the mapping from a bimodal to a Gaussian. The SAR method easily handles the bimodal $f(x)$ and the highly non-linear $u(x)$.

Figure 4. In the same format as Figure 1, this depicts the mapping from a stretched exponential to a Gaussian. The divergence in $f(x)$ does not prevent the SAR method from recovering $u(x)$.

Figure 5. The constructed $F^*(x)$ and $G^*(y)$ are plotted on the same horizontal axis. We have assumed only 15 samples from X and 25 samples from Y . The width $2\Delta y$ represents the uncertainty in the estimates of $Y = u(X)$. The estimation error grows in the tails of the distributions, owing to under-sampling of the low probability density.

Figure 6. Two approximations to the true $u(X)$ show the effect of noisy samples. In this simulation, the SAR approximation is actually closer to the true $u(X)$ than a simultaneous regression.

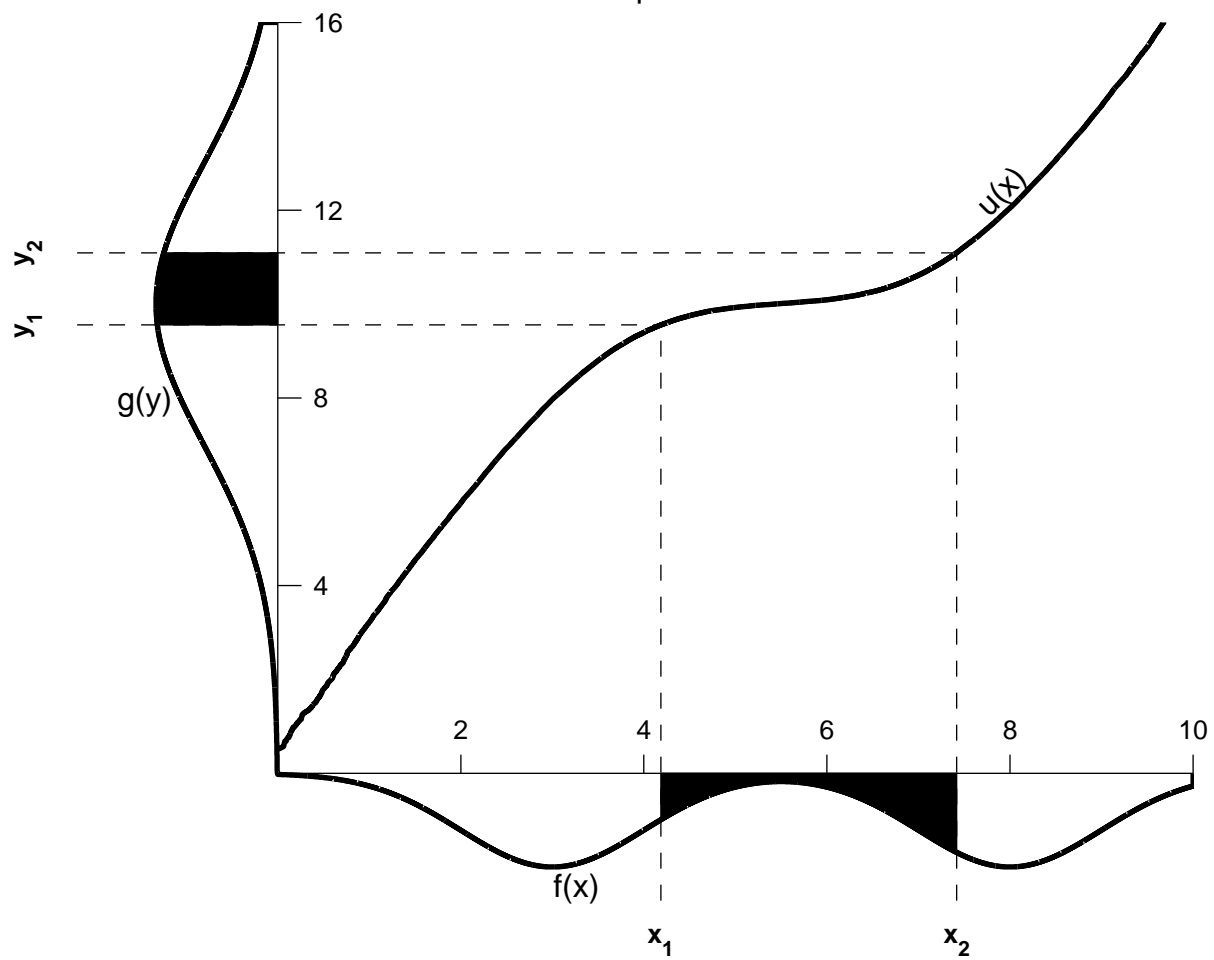
Figure 7. The distributions of values of α in $u(x) = \beta e^{\alpha x}$ obtained from two regression methods. For this example, the SAR method typically produces a better α than a standard simultaneous regression.

Figure 8. The median estimated α in $u(x) = \beta e^{\alpha x}$ for two regression methods. The SAR estimate quality drops more slowly than that of the simultaneous regression.

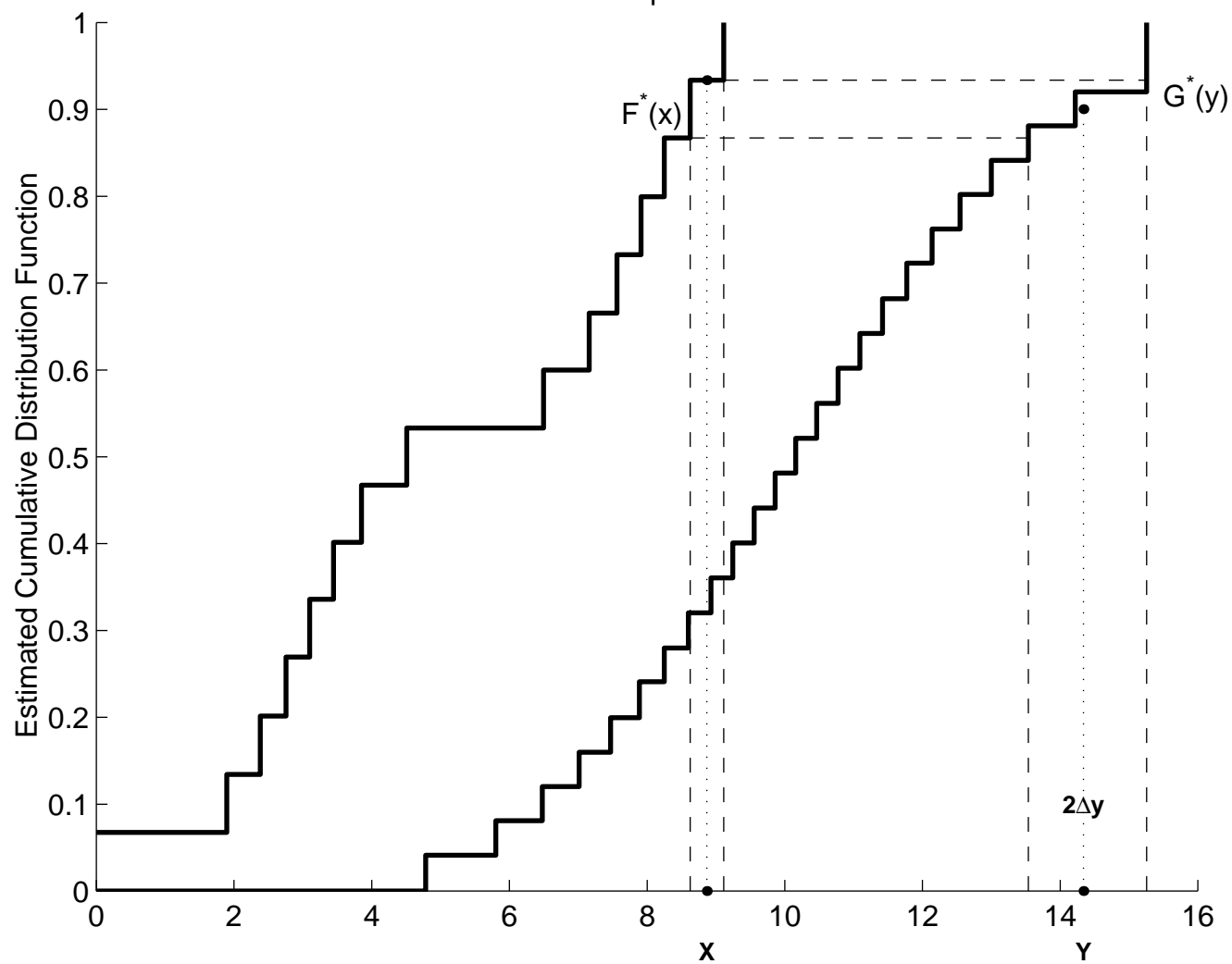
Figure 9. This plot depicts estimated complementary CDFs for X and Y . Note that the vertical axis is logarithmic and the horizontal axis is to the $\frac{1}{2}$ power. The solid lines represent the tabular forms of the CDFs and the dashed lines depict the analytical fits with equations (43) and (44).

Figure 10. The figure shows the tabular and analytical representations of the mapping function from dawn flux to noon flux. It is impossible to obtain this function using simultaneous measurements because GOES 8 is never both at dawn and at noon. The crosses through each dot have been exaggerated to indicate $\pm 3\Delta x$ and $\pm 3\Delta y$ as calculated by (37) and (36). The plot indicates a simple proportional mapping from X to Y , which is physically very reasonable.

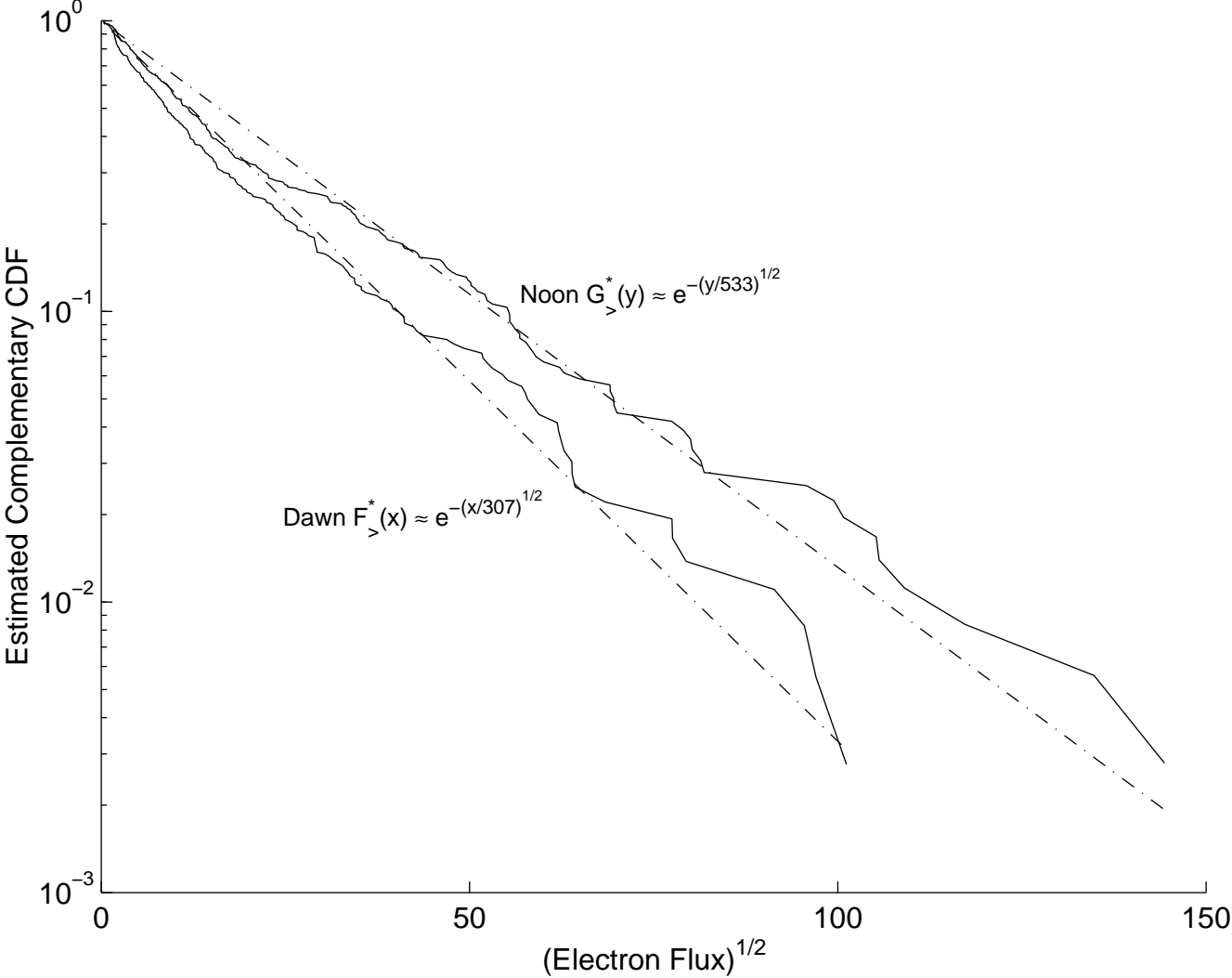
Bimodal Example PDFs



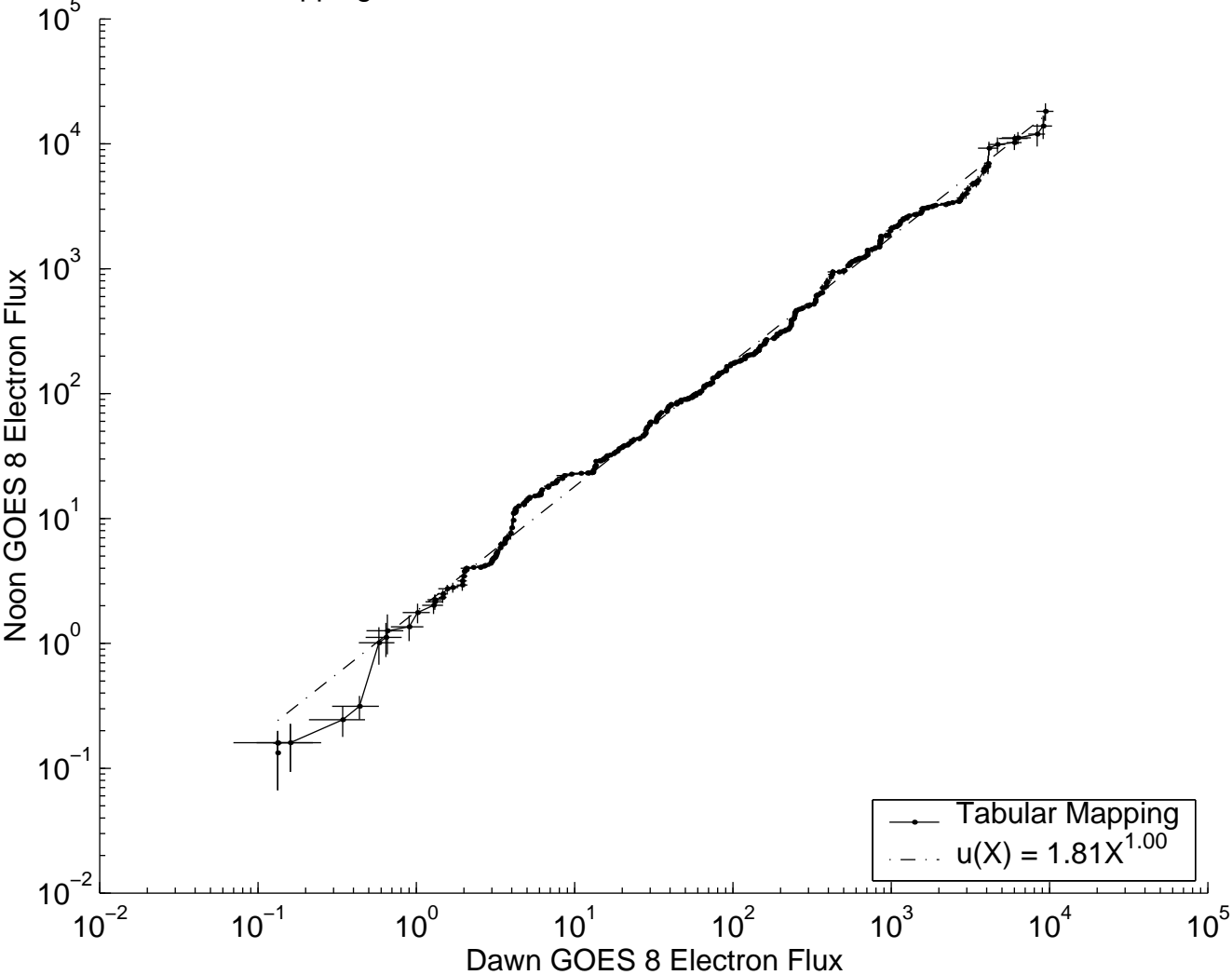
Bimodal Example Estimation



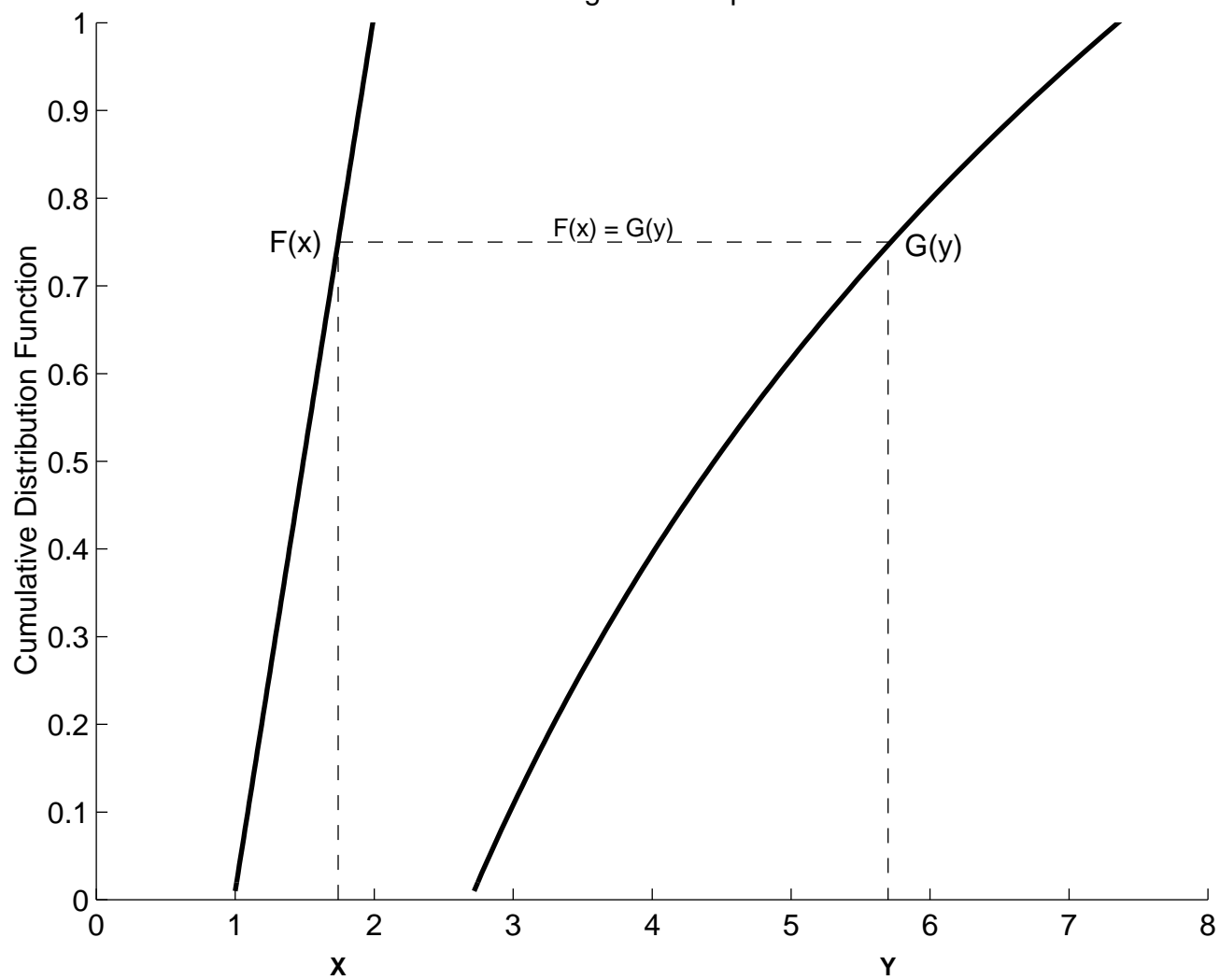
Distribution of GOES 8 Electron Flux from Local Dawn and Noon



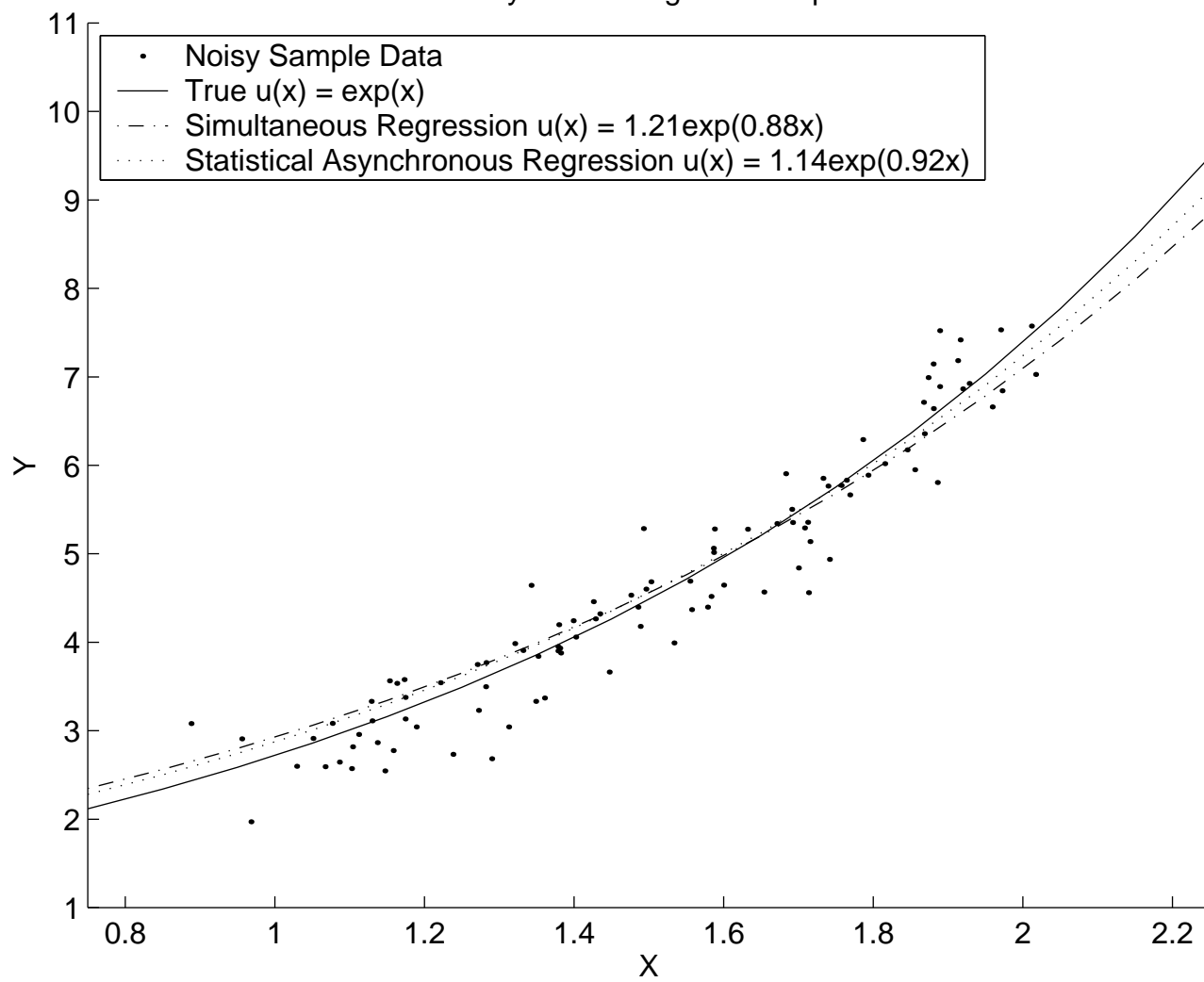
Mapping of GOES 8 Electron Flux from Local Dawn to Noon



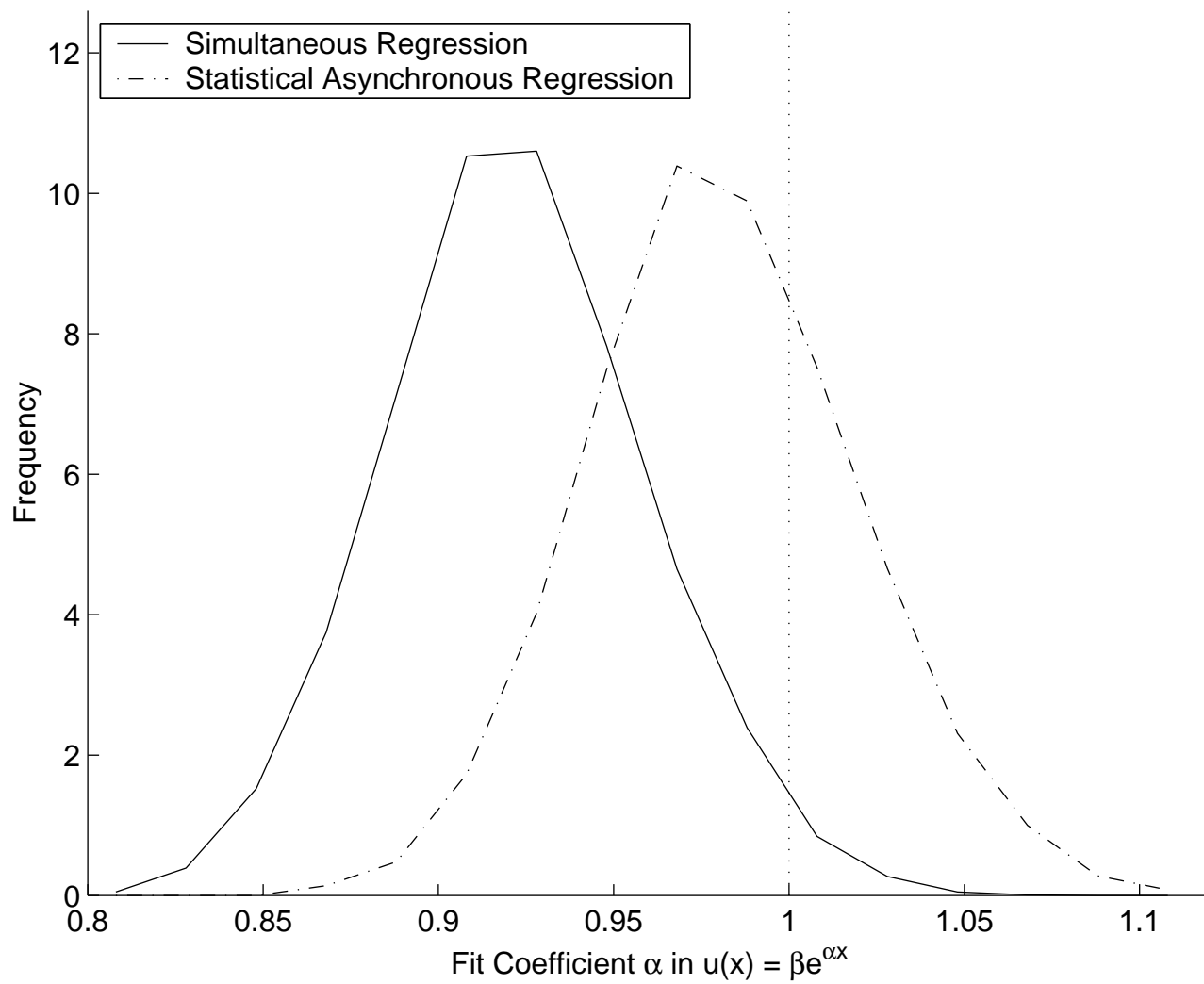
Meteorological Example CDFs



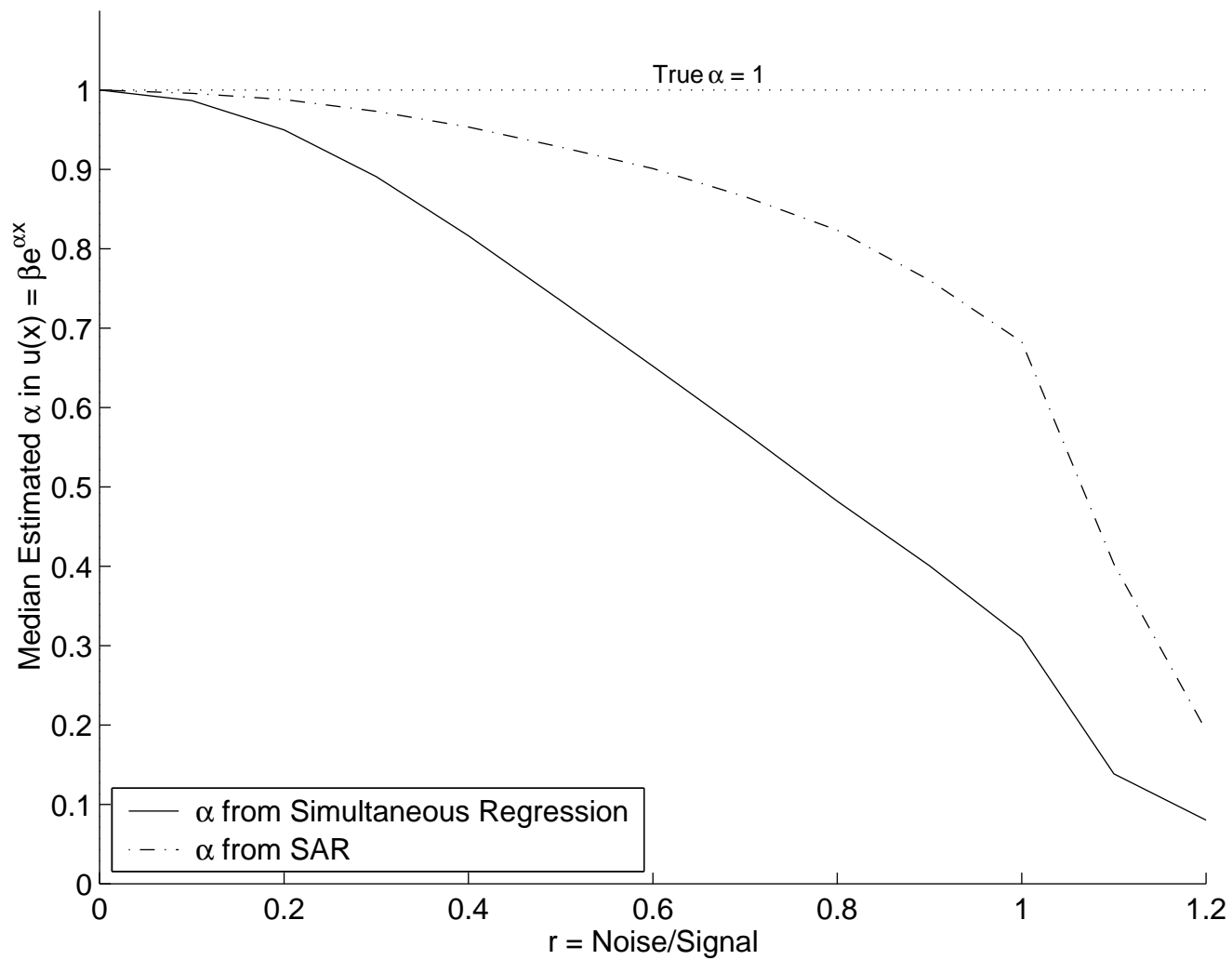
Noisy Meteorological Example



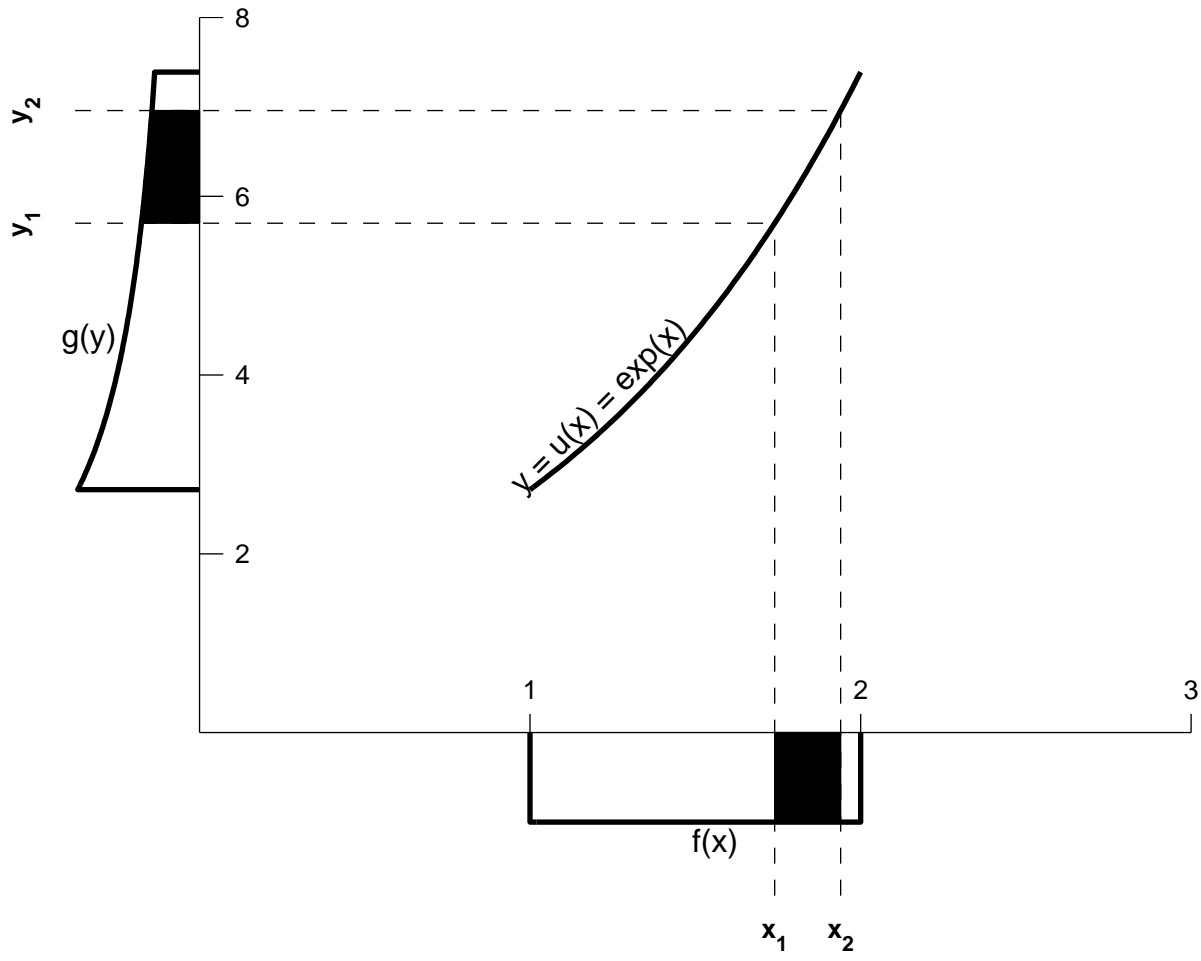
Distribution of Coefficient α for Two Fitting Methods



The Dependence of Estimation Quality on Noise Amplitude



Meteorological Example PDFs



Stretched Exponential Example : $u(X) = 2X^{1/2}$

